48th AIAA Aerospace Sciences Meeting Including the New Horizons Forum and Aerospace Exposition
4 - 7 January 2010, Orlando, Florida


# Physics Based Analysis of Horseshoe Plasma Actuator for Improving Film Cooling Effectiveness

Chin-Cheng Wang* and Subrata Roy§
*Computational Plasma Dynamics Laboratory and Test Facility*
*Mechanical and Aerospace Engineering Department*
*University of Florida, Gainesville, FL 32611-6300*

**We numerically test horseshoe plasma actuator for film cooling enhancement in gas turbines. We solved three-dimensional plasma governing equations using finite element based MIG flow code instead of using phenomenological model or reduced order model as before. Two problems are considered in the present study. The first problem is to find the best case of using horseshoe plasma actuator for improving film cooling. The second problem is to simulate a turbine case of a single row of 35 degree round holes on a flat plate from Sinha's experiment. We utilize the electric force density which is calculated from plasma governing equations for effective flow control. Such electric force induces attachment of cold jet to the work surface by actively altering the body force in the vicinity using a horseshoe plasma actuator. We have shown a progressive improvement of centerline effectiveness as the electric force density increases from 0 (no force) to 8 MN/m$^3$ (maxima). Fluid flow predictions with finite volume based simulation are performed using standard turbulence models. All the cases are simulated here for a unit blowing ratio. Results are compared with the published experimental data and other numerical predictions for the latest film cooling technology to identify effectiveness improvement. The numerical results show an improvement of effectiveness well above 100% over the standard baseline design.**

## Nomenclature

| | | |
|---|---|---|
| $D_{e,i}$ | = | electron or ion diffusion coefficient (cm$^2$/s) |
| $d$ | = | circular pipe diameter (mm) |
| $E$ | = | electric field (V/m) |
| $e$ | = | elementary charge (C) |
| $F$ | = | electric force density (N/m$^3$) |
| $k_B$ | = | Boltzmann's constant (J/K) |
| $M$ | = | blowing ratio, $\rho_j V_j/\rho_f V_f$ |
| $n_{e,i}$ | = | electron or ion density (m$^{-3}$) |
| $p$ | = | pressure (Torr) |
| $q$ | = | charge separation, $n_i$-$n_e$ (m$^{-3}$) |
| $r$ | = | recombination rate (cm$^3$/s) |
| $T$ | = | local static temperature (K) |
| $V$ | = | gas velocity (m/s) |
| $\alpha_a$ | = | jet issuing angle (degree) |
| $\alpha$ | = | Townsend coefficient (cm$^{-1}$) |
| $\varepsilon_0$ | = | vacuum permittivity (F/m) |
| $\phi$ | = | potential (V) |
| $\eta$ | = | film cooling effectiveness, $(T_{fs}$-$T_s)/(T_{fs}$-$T_j)$ |
| $\Gamma_e$ | = | electron flux (m$^{-2}$ s$^{-1}$) |
| $\mu_{e,i}$ | = | electron or ion mobility (cm$^2$/sV) |
| $\rho$ | = | gas density (kg/m$^3$) |

* Research Scientist, Member AIAA, james614@ufl.edu
§ Associate Professor, Associate Fellow AIAA, roy@ufl.edu

## I. Introduction

Crossflow jets have been widely used in many engineering problems, such as film cooling for gas turbine blades. Gas turbine blades suffer from very high thermal stresses due to hot effluent gases from the combustion chamber. The problem worsens with increasing turbine inlet temperature for higher thermal efficiency of gas turbine engine. Repetitive thermal stress over a long duration significantly affects the lifetime of turbine blades. There are numerous methods of turbine blades cooling for increasing the lifetime. Film cooling is one of the most promising methods to inject cold jets through rows of surface holes located in the spanwise direction. The resultant penetration of the cold jets into the hot freestream gas forms a thin film for protecting blade surfaces from thermal stress. However, for realistic problem at certain blowing ratio (i.e., momentum ratio of injected air to crossflow), the attachment of the cold jets to the wall is crucial due to the lift-off effect. Haven and Kurosaka[1] examined the effect of hole exit geometry on the near field characteristics of crossflow jets. They found that the nascent streamwise vortices evolve eventually into kidney shape vortices downstream. From the experimental observation, we can see the lift-off behavior of the kidney vortices is formed as the cold jet interacts with the hot freestream gas shown in figure 1.

Tons of numerical simulations of improving cooling performance by reducing lift-off effect have been studied. Our prior publication[2] showed an optimum hole spacing and low issuing angle for maximum cooling efficiency. Walters and Leylek[3] provided a understanding of the flow physics for different film hole length to diameter ratio and blowing ratio with cylindrical cooling holes. Hyams *et. al.*[4], Azzi *et. al.*[5], and Zhang *et. al.*[6] presented different shaped holes for detailed analysis of film cooling physics. Results indicated that changes in film cooling hole shape can strongly affect the downstream behavior of the film. Na and Shih[7] proposed a ramp modification at upstream of the holes to modify the interaction of incoming flow and cooling jet. Results showed ramp design gives two times higher laterally averaged effectiveness than without the ramp.

For more accurate turbine blade simulation, Garg[8] and Heidmann *et. al.*[9] considered realistic film-cooled turbine vane geometry including the plenum and hole pipes with Wilcox's $k$-$\omega$ turbulence model. These studies provide good details of the flow. However, the anisotropic dynamic nature of the spanwise vortices that affect the film cooling process are more complex than that can be captured by the mixing models used in aforementioned papers. The two competing factors important for any turbulence model are accuracy and efficiency (i.e. computational cost). An optimal combination of both these factors is hard to achieve and thus, the primary purpose of the numerical simulation is towards attaining such a goal. People suggest using large eddy simulation (LES) or direct numerical simulation (DNS) to capture minor flow details. Zhong and Brown[10] conducted DNS for solving a 3-dimensional multi-hole cooling problem. The computed cooling effectiveness showed good agreement with experimental results for low blowing ratio cases. However, DNS and LES are computationally limited for high Reynolds number flow. As a remedy, a detached eddy simulation (DES) turbulence model is wildly published for capturing better description of the dynamic flow structures. Kapadia *et. al.*[11], Martini *et. al.*[12], and Kim *et. al.*[13] investigated film cooling flow with unsteady DES. Results indicate that the mixing processes downstream of the hole are highly anisotropic, as the turbulent diffusion is much stronger in the transverse direction.

Several experimental efforts[14-16] have been documented in the literature. Sinha *et. al.*[14] provided thorough experimental data for film cooling effectiveness with different density ratio and blowing ratio on a flat plate of a row of inclined holes. The results showed the centerline effectiveness scaled with the mass flux ratio and laterally averaged effectiveness dependent on density ratio and momentum flux. Bell *et. al.*[15] presented five different shaped holes for different blowing ratios, momentum flux ratios, and density ratios. Some of these designs increase lateral spreading. Bunker[16] also provided a review of the shaped holes for film cooling. He summarized the benefits of shaped hole such as higher centerline and spanwise effectiveness than round hole and little variation in effectiveness over blowing ratio from 0.5 to 2. Ekkad *et. al.*[17] investigated jet pulsing frequencies of 5 Hz to 20 Hz and duty cycle at different level of 10% to 100% on film effectiveness for different blowing ratios from 0.25 to 2. Results indicate the higher effectiveness and lower heat transfer coefficients are obtained at the reduced duty cycles. For detailed discussion of analyses methodologies, physical descriptions, and various influences on film cooling performance, Bogard and Thole[18] provided thorough review in the literature. It was found that there are strong effects of freestream turbulence, surface curvature, and hole shape on the performance of film cooling.

The complex dynamic nature of the film cooling flow makes it necessary to actively control it with a dynamic force that varies temporally and spatially working with the dominant turbulence scales. In our prior publications[19,20],

we proposed a concept using plasma electric force to actively enhance interaction of cool air jets with hot crossflow for improved cooling of hot surfaces. Hot freestream gas will enhance dissociation and hence help plasma generation due to ionization in the vicinity of the electrodes. Both pulsed dc and ac powered plasma actuators can induce such active control over the dynamics of film cooling. The momentum transfer between the plasma and gas happens due to collisional momentum transfer between charged ions and neutral atoms. Such actuation of the flow is active and near instantaneous, does not require any mechanical parts, and the actuator electrode sets can be applied as a patch on the surface of the existing ceramic coating of the turbine blade or embedded into the coating. There could be practical considerations like surface oxidation of the electrodes and spallation. In the present study, we solve plasma governing equations to model the physics of plasma horseshoe actuator instead of using the phenomenological model or the reduced order model. The electric force density is calculated from multiplication of electric field and charge separation and is located just downstream of the cooling hole exit. While in practical situation this force will be transient, we consider the time averaged of the electric force as a local body force term in Navier-Stokes equations. This is allowable due to largely disparate timescales of plasma and gas flow.

## II. Problem Descriptions

For the first problem, we consider three different cases with and without plasma force on the flat plate shown in the figure 2. Here we place a horseshoe plasma actuator at the downstream of the coolant hole for the test case two and three. Such actuators are made of a set of electrode pairs between which electric potential induced weak ionization of the working gas generate an electric body force that is dominant inside the boundary layer. We can easily power inner or outer electrode to create different directions of electric force. In such an actuator the flow actuation is directly linked with the gas-charged particle interaction and thus instantaneous. Figure 3 shows the top view and the side view of the electrode layout and boundary condition setup. In this case, such setup will create an inward electric force, and it may reduce the jet momentum coming out from the coolant hole.

After we find the best case from above test cases, the second problem will apply the plasma electric force for the benchmark case from Sinha *et. al.*[14]. Figure 4 describes schematic control volume of freestream air passing over a flat surface (e.g., a turbine blade). This surface of study has a row of injection holes through which the cool air is issued at an angle $\alpha_a = 35°$. The cool jet at temperature $T_j = 150$ K is injected into the hot freestream of $T_{fs} = 300$ K. The injection ducts are circular pipes with diameter equal to $d = 2.54$ mm. The injection hole formed by the intersection of the injection pipe with the wind tunnel is an ellipse with the minor and the major axes $d$ and $D = d/(\sin\alpha)$, respectively. The distance between the hole centers is $L = 3d$. The selected mean flow velocities, static pressures and temperatures (i.e., densities) in the injection pipe and the wind tunnel gives a blowing ratio $M = 1$. The inlet section is located at $x = -20d$ and the exit is located at $x = 29d$. The other dimensions and boundary conditions are shown in the figure 4. The flat (blade) surface is considered adiabatic. The actual plasma electric force density is measure to be ~kN/m$^3$ which consumes tens of watts of power.[21] However, such small actuation may not be useful to control the cold jet to attach to the actual turbine blade surface. The electric force density has to be three orders of magnitude higher than the standard plasma actuator. Such higher force density (~MN/m$^3$) will only utilize a small fraction of power (less than 1% of the turbine power) for such arrangement which may eventually reduce the energy budget by more effective cooling.

An important parameter for comparing film cooling performance is its effectiveness $\eta = (T_{fs} - T_s)/(T_{fs} - T_j)$, where $T_s$, $T_j$ and $T_{fs}$ are the work surface, cooling jet and freestream gas temperatures, respectively. The effectiveness is plotted against a non-dimensional ratio $x/Md$, where $x$ is the downstream distance, $M = \rho_j V_j/\rho_{fs} V_{fs}$ is the blowing ratio, and $d$ is the circular pipe diameter. The density $\rho_j$ and velocity $V_j$ of the fluid at the jet exit plane are related to the freestream density $\rho_{fs}$ and velocity $V_{fs}$ such that $\rho_j/\rho_{fs} = MV_{fs}/V_j$.

## III. Numerical Method

### A. Governing equations

A hydrodynamic model is obtained from Kumar and Roy[22] for multi-scale plasma discharge simulation. The model uses an efficient finite element algorithm. The unsteady transport for electrons and ions is derived from fluid

dynamics in the form of mass and momentum conservation equations. The species momentum is modeled using the drift-diffusion approximation under isothermal condition that can be derived from the hydrodynamic equation. The continuity equations for ion and electron number densities and Poisson equation are given by:

$$\frac{\partial n_i}{\partial t} + \frac{\partial}{\partial x_j}\left\{ n_i \mu_i E_{x_j} - D_i \frac{\partial n_i}{\partial x_j} \right\} = \alpha \left|\Gamma_e\right| - r n_i n_e \tag{1}$$

$$\frac{\partial n_e}{\partial t} + \frac{\partial}{\partial x_j}\left\{ -n_e \mu_e E_{xj} - D_e \frac{\partial n_e}{\partial x_j} \right\} = \alpha \left|\Gamma_e\right| - r n_i n_e \tag{2}$$

$$\nabla \cdot (\varepsilon_0 E) = -e(n_e - n_i) \tag{3}$$

where $n_{i,e}$ is the number density, $\mu_{i,e}$ is the mobility, $E$ is the electric field, $D_{i,e}$ is the diffusion, $\left|\Gamma_e\right|$ is the effective electron flux and depends mainly on the electric field, $r$ is the electron-ion recombination rate, $\varepsilon_0$ is the permittivity in vacuum, $e$ is the elementary charge of $1.6022\times10^{-19}$ C, subscript $j$ is the coordinate direction, subscript $i$ and $e$ are ion and electron, respectively, and $q = n_i - n_e$ is the charge separation. The discharge is maintained using a Townsend ionization scheme. The ionization rate is expressed as a function of Townsend coefficient $\alpha$:

$$\alpha = Ap \exp\left[-B/(\left|E\right|/p)\right] \tag{4}$$

where $A$ and $B$ are preexponential and exponential constants, respectively, $p$ is the gas pressure. The system of equations (1)-(3) is normalized using the following normalization scheme: $\tau = t/t_0$, $x_j^* = x_j/d_l$, $N_e = n_e/n_0$, $N_i = n_i/n_0$, and $\phi = e\,\varphi/k_B T_e$ where $t_0$ is the reference time of $10^{-8}$ s, $d_l$ is usually a domain characteristic length in the geometry, $n_0$ is the reference density of $10^{15}$ m$^{-3}$, $k_B$ is the Boltzmann's constant, and $T_e$ is the electron temperature. The working gas is nitrogen. The ion mobility and diffusion at 300 K as well as electron mobility and diffusion at 11600 K are given by Surzhikov and Shang[23].

We apply the time average of the electric force density ($\mathbf{F} = e\mathbf{E}q$) in the Navier-Stokes equations as a local body source term for an incompressible Newtonian fluid shown below:

$$\rho \nabla \cdot \mathbf{V} = 0 \tag{5}$$

$$\rho \frac{D\mathbf{V}}{Dt} = -\nabla p + \rho \mathbf{f} + \mu \nabla^2 \mathbf{V} \tag{6}$$

$$\rho \frac{DE_T}{Dt} = -p \nabla \cdot \mathbf{V} + k \nabla^2 T \tag{7}$$

where $\rho$ is the gas density, $\mathbf{V}$ is the gas velocity, $\mathbf{F} = \rho\mathbf{f}$ is the electric force density, $\mu$ is the gas viscosity, and $E_T$ is the total energy.

### B. Computational approach and boundary condition

A finite element method (FEM) based module driven Multi-scale Ionized Gas (MIG) flow code has been utilized for solving three dimensional plasma governing equations for all problems. MIG flow code has been verified and utilized for many applications. Computed solutions show details of the distribution of charged and neutral particles and their effects on the flow dynamics. The forward temporal evolution is evaluated using the fully implicit ($\theta = 1$) time stepping procedure. The Newton-Raphson scheme is used for dealing with nonlinear terms. To solve the sparse matrix, we apply an iterative sparse matrix solver called Generalized Minimal RESidual (GMRES). The assembly procedure involves storing only the non-zero elements of the Jacobian matrix in the form of a linear array and the corresponding row and column locations using an incremental flag. The solution is assumed to have converged when the $L_2$ norms of all the normalized solution variables and residuals are below a chosen convergence criterion of $10^{-3}$.

For the first problem, the complete plasma kinetics and fluid dynamics are solved using MIG in a consistent fashion. We test three different cases using MIG for improving film cooling shown in figure 2. In test case #1

without plasma force, hot freestream comes from $x$-direction with uniform velocity of 0.3 m/s and temperature of 300 K. The cold jet comes from a coolant hole and injects to the bulk with an angle of 45º, velocity of 0.42 m/s and temperature of 150 K. The fluid boundary condition can be found in figure 3. We employ velocity inlet at $x = 0$ and $x = 0.3$ mm, and zero pressure outlet at $x = 0.6$ mm. Symmetry boundaries are maintained at $y = 0$, $y = 0.6$ mm, and $z = 0.24$ mm. At the bottom wall, an adiabatic wall boundary condition with no-slip is imposed. In the test case #2 with plasma outward force, horseshoe plasma actuator is placed just slightly downstream of the coolant hole. For plasma boundary conditions, we power the inner electrode of 50 V and ground the outer electrode of 0 V. The ion density is maintained zero at powered electrode and the electron density is maintained zero at grounded electrode. The last test case #3 with plasma inward force is shown in the figure 3. We simply power outer electrode (red) and ground the inner electrode (black). All the boundary conditions are maintained the same just like we stated above.

For the second problem shown in the figure 4, at the freestream inlet $x = -20d$, an injected mass flow rate inlet condition was applied with the density ratio of $\rho_j/\rho_{fs} = 2$, velocity ratio of $V_j/V_{fs} = 0.5$, and turbulent intensity of 5%. At the exit plane $x = 29d$, the gauge pressure at the outlet boundary is maintained at 0 Pa. The work surface is an adiabatic wall with a single row of holes through which cool air at temperature is equal to $T_j = 150$ K is injected at an angle of $\alpha = 35º$ into the freestream temperature $T_{fs} = 300$ K. The domain extends from the plenum base at $z = -6d$ to $z = 20d$ from work surface where a pressure-far-field boundary condition was applied. The periodic boundary condition was applied in the crosswise direction (at $y = \pm 1.5d$) in the computational domain. For the coolant plenum, we applied no-slip wall condition on $x/d = -14$ and 8, and $z/d = -2$ surfaces; mass flow inlet condition for $z/d = -6$. The established EHD force data computed by MIG is applied to solve the three-dimensional fluid dynamics using a commercial CFD package, FLUENT™ 6.3.26. The flow is assumed compressible and turbulent. The Reynolds number based on hole diameter and inlet conditions was 16100. A maximum Mach number not exceeding 0.3 was achieved in the flow field while maintaining the desired Reynolds number by scaling the experimental geometry down by a factor of 5. This resulted in a hole diameter of 2.54 mm, and was done to allow more rapid convergence of the solution using the density-based formulation of the computer code while minimizing compressibility effects. We interpolate the time-averaged electric force density as a source term in the momentum equations using user defined functions (UDF). We use the ideal gas approximation and the Advection Upstream Splitting Method (AUSM) solver closed with ReNormalized Group (RNG) $k$-$\varepsilon$ turbulence model with standard wall function. The courant number was set equal to 1 for solution control. A second-order upwind discretization method is used. Convergence is determined when the residual among the continuity, momentum, energy, turbulent kinetic energy, and turbulent dissipation are less than $10^{-3}$. The density of computational mesh of ~200,000 cells was tested and verified in our prior publications[19,20]. It is well known that coarse grids cannot resolve the effect of the downstream vortices. All the simulations take ~1400 iterations for convergence. Depending on the actuation device a local kN/m$^3$ force density may be obtained with a few input watts[21]. For the actual gas turbine, it may require force density of MN/m$^3$ which costs kW level power of consumption for effective flow control.

## IV. Results and Discussion

Two problems are investigated in this paper. The first one is three different test cases with and without horseshoe plasma actuator, and the other is benchmark case from Sinha *et. al.*[14] with scaled plasma force density for improving film cooling effectiveness. Since we used an inherently time averaged turbulence model for benchmark case, computed results were presented at the steady state. For blowing ratio $M = 1$, a combination of flow profiles at the wind tunnel and cold jet inlet is very complex. This is due to the fact that at this range of velocities existing in the pipe, the boundary layers are not thin everywhere in the pipe. At very thick boundary layers, the flow close to the wall behaves as a typical boundary layer, while for very thin incoming boundary layers a wall-jet flow exists downstream the jet exit. Such flow motion creates a bound kidney shaped vortical structure that stretches downstream along the primary flow direction. Details of such structure are available in our previous publication.[2,11]

### A. First problem

Three different cases are shown in figure 2. The temperature distribution of the test case one without plasma force is shown in figure 5. We can see the hot freestream of 300 K interacts with cold jet of 150 K at ($x$, $y$) = (0.3, 0.3 mm). We can see that the attachment of cold fluid protects the downstream surface. This baseline case is used

for comparing with plasma actuation effect for other two cases. In the test case two, we power the inner electrode of the horseshoe actuator. We can see the electric force vectors distribution overlay on the figure 6(a) charge separation at *xz*-plane ($y$ = 0.3 mm) and potential distribution at *xy*-plane ($z$ = 0.03 mm). The force is acting outward from powered electrode to the grounded electrode in three dimensions. The peak of charge separation is ~$10^{15}$ $m^{-3}$. The potential varies from 50 to 0 V which is balanced between electric field and charge separation from Poisson equation. The force density for this electrode arrangement (not shown) is in the order of $kN/m^3$. In such force density actuation around the cold jet, the temperature profiles are shown in the figure 6(b). We can see such force actuation drastically change the flow path of the cold jet upward. From the top view of the work surface at $z$ = 0.3 mm, it is easily to see high temperature (above 290 K) at downstream of the coolant hole. For the last test case, we power the outer electrode of the horseshoe plasma actuator. The powered electrode is colored in red and the grounded electrode is marked in black showing in the figure 7(a). We can see that an inward plasma force is created. Such force reduces the jet momentum and increases the film cooling effectiveness at the downstream of coolant hole shown in the figure 7(b). From the above test cases, we can see the last case is helpful in attaching the cold jet to the work surface and increasing the film cooling effectiveness in both streamwise and spanwise directions.

### B. Second problem

In the benchmark case with higher blowing ratio, standard plasma actuator is limited by small actuation effect. It has been proven to be effective at low speed ~20m/s. For blowing ratio of one with jet flow speed of 50 to 100 m/s, we need to scale the force density from $kN/m^3$ to $MN/m^3$ for effective flow control. Figure 8(a) plots the temperature distribution on the vertical mid-plane ($y$ = 0), while figure 8(b) shows the temperature distribution on the horizontal work surface ($z$ = 0). Seven cases are simulated with force density varied from an initial zero (no force) to a maximum of 8 $MN/m^3$. It is obvious that the lift-off effect causes a significant reduction in effectiveness for the baseline case (i). As we increase the force density, the flow completely attaches to work surface. Importantly, the actuation force applied in a three-dimensional manner demonstrates successful spreading of the cold film over the downstream surface not only in the streamwise direction but also in the crosswise fashion. As the force density increases shown in figure 8(b), the cold flow attachment has significant effect near the coolant hole.

Figure 9 plots the centerline effectiveness at downstream of the coolant hole. The computed centerline results for the baseline case (no force) compares reasonably with the experiment of Sinha *et al.*[14] and two other previously reported numerical results[24-25]. We can see the centerline effectiveness decreases for the baseline case as the distance of downstream (X/d) increases due to the lift-off effect. As the force density increases to the maximum, the centerline effectiveness increases by over 100% than the baseline case.

## V. Conclusion

We solve the plasma governing equations and Navier-Stokes equations using finite element based MIG flow code and finite volume based Fluent™ 6 for gas turbine blade. Two problems are introduced in the present study for improving film cooling. For the first problem, we test three different cases to find a higher film cooling effectiveness on the work surface. Based on the temperature distribution, test case three with plasma inward force has a significant jet attachment to the wall at downstream of coolant hole. The force density of the horseshoe actuator is measured ~$kN/m^3$ which costs few watts of power. In benchmark case (blowing ratio larger than one), the force density of $MN/m^3$ is required for the effective flow control. So we vary and utilize the electric force density from 0 (no force) to 8 $MN/m^3$ in the second problem. We can see a tremendous improvement of film cooling effectiveness for both streamwise and spanwise direction than a baseline case. The baseline case was compared with experimental data and other numerical works with a good agreement. The improvement of centerline effectiveness is above 100% than a baseline case when the force density increases to the maxima. The hybrid DES and/or LES type turbulence model will possibly be better to capture such complex flow structures, but it will also take much computational costs. Plasma augmented design modified flow control ideas may become more beneficial for cases with badly separated jets at higher velocity ratio. Realistic experimentation is underway to valid these numerical data.

## Acknowledgments

This work was partially supported by the AFOSR Grant FA9550-09-1-0004 monitored by Dr. John Schmisseur and the FCAAP grant.

## References

[1]B.A. Haven and M. Kurosaka, "Kidney and anti-kidney vortices in crossflow jets," *Journal of Fluid Mechanics*, 352, 1997, pp. 27-64.

[2]S. Roy, "Numerical investigation of the blade cooling effect by multiple jets issuing at an angle," *Numerical Heat Transfer – Part A*, 38 (7), 2000, pp. 701-718.

[3]D.K. Walters and J.H. Leylek, "A detailed analysis of film cooling physics: Part I— Streamwise injection with cylindrical holes," *Journal of Turbomachinery*, 122, 2000, pp. 102-112.

[4]D.G. Hyams and J.H. Leylek, "A detailed analysis of film cooling physics: Part III— Streamwise injection with shaped holes," *Journal of Turbomachinery*, 122, 2000, pp. 122-132.

[5]A. Azzi and B.A. Jubran, "Numerical modeling of film cooling from converging slot-hole," *Heat Mass Transfer*, 43, 2007, pp. 381-388.

[6]X.Z. Zhang and I. Hassan, "Film Cooling Effectiveness of an Advanced-Louver Cooling Scheme for Gas Turbine," *J. Thermophys. Heat Transfer*, 20 (4), 2006, pp. 754-64.

[7]S. Na and T.I-P. Shih, "Increasing adiabatic film-cooling effectiveness by using an upstream ramp," *Journal of Heat Transfer*, 129, 2007, pp. 464-471.

[8]V.K. Garg, "Heat transfer on a film-cooled rotating blade," *Int. J. Heat and Fluid Flow*, 21, 2000, pp. 134-145.

[9]J.D. Heidmann, D.L. Rigby and A.A. Ameri, "A three-dimensional coupled internal/external simulation of a film-cooled turbine vane," *Journal of Turbomachinery*, 122, 2000, pp. 348-359.

[10]F. Zhong and G.L. Brown, "A 3-dimensional, coupled, DNS, heat transfer model and solution for multi-hole cooling," *Int. J. Heat and Mass Transfer*, 50, 2007, pp. 1328-1343.

[11]S. Kapadia, S. Roy and J. Heidmann, "First hybrid turbulence modeling for turbine blade cooling," *Journal of Thermophysics and Heat Transfer*, 18 (1), 2004, pp. 154-156.

[12]P. Martini, A. Schulz and H.-J. Bauer, "Derached eddy simulation of film cooling performance on the trailing edge cutback of gas turbine airfoils," *Journal of Turbomachinery*, 128, 2006, pp. 292-299.

[13]S.I. Kim and I.G. Hassan, "Unsteady heat transfer analysis of a film cooling flow," AIAA-2008-1287.

[14]A.K. Sinha, D.G. Bogard and M.E. Crawford, "Film-cooling effectiveness downstream of a single row of holes with variable density ratio," *Journal of Turbomachinery*, 113, 1991, pp. 442-449.

[15]C.M. Bell, H. Hamakawa and P.M. Ligrani, "Film cooling from shaped holes," *Journal of Heat Transfer*, 122, 2000, pp. 224-232.

[16]R.S. Bunker, "A review of shaped hole turbine film-cooling technology," *Journal of Heat Transfer*, 127, 2005, pp. 441-453.

[17]S.V. Ekkad, S. Ou and R.B. Rivir, "Effect of jet pulsation and duty cycle on film cooling from a single jet on a leading edge model," *Journal of Turbomachinery*, 128, 2006, pp. 564-571.

[18]D.G. Bogard and K.A. Thole, "Gas turbine film cooling," *Journal of Propulsion and Power*, 22, 2006, pp. 249-270.

[19]S. Roy and C.-C. Wang, "Plasma actuated heat transfer," *Applied Physics Letters*, 92, 231501, 2008.

[20]C.-C. Wang and S. Roy, "Electrodynamic enhancement of film cooling of turbine blades," *Journal of Applied Physics*, 104, 073305, 2008.

[21]J.W. Gregory, C.L. Enloe, G.I. Font, and T.E. McLaughlin, "Force production mechanisms of a dielectric-barrier discharge plasma actuator," AIAA-2007-185.

[22]H. Kumar and S. Roy, "Multidimensional hydrodynamic plasma-wall model for collisional plasma discharges with and without magnetic field effects," *Physics of Plasmas* 12, 093508, 2005.

[23]S.T. Surzhikov and J.S. Shang, "Two-component plasma model for two-dimensional glow discharge in magnetic field," *Journal of Computational Physics* 199, 2004, pp. 437-464.

[24]A.A. Immarigeon, "Advanced Impingement/ Film-Cooling Schemes for High-Temperature Gas Turbine—Numerical Study," M.Sc. Thesis, Concordia Univ., Montreal, 2004.

[25]K. B. Mulugeta, and S. V. Patankar, "A Numerical Study of Discrete-Hole Film Cooling," ASME Paper 96-WA/HT-8, 1996.

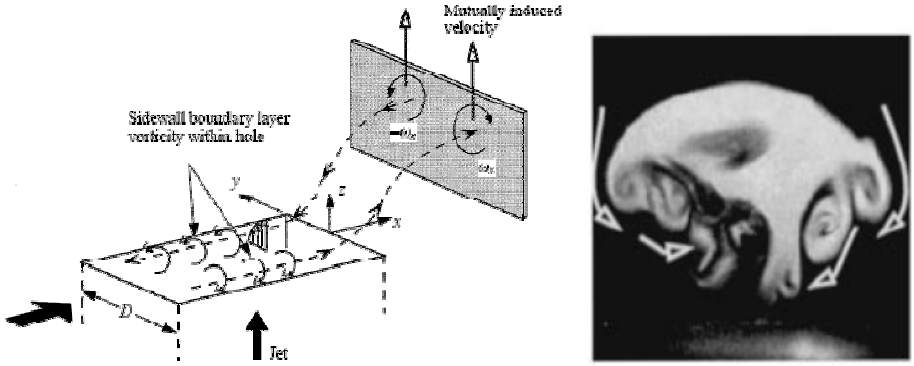


(a) (b)

**Figure 1. Schematic shows (a) kidney vortices due to hole sidewall vorticity. (b) Kidney vortices at downstream of coolant hole with elliptic hole geometry.[1]**

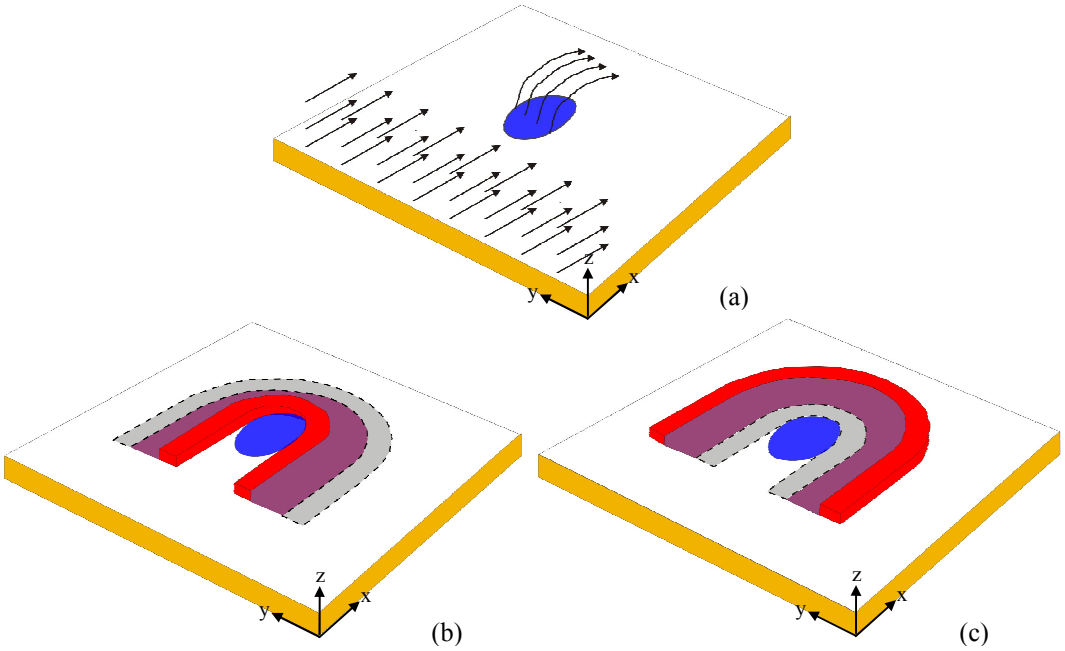


**Figure 2. Schematic shows the film cooling flow for (a) without plasma force, (b) with plasma outward force, and (c) with plasma inward force.**

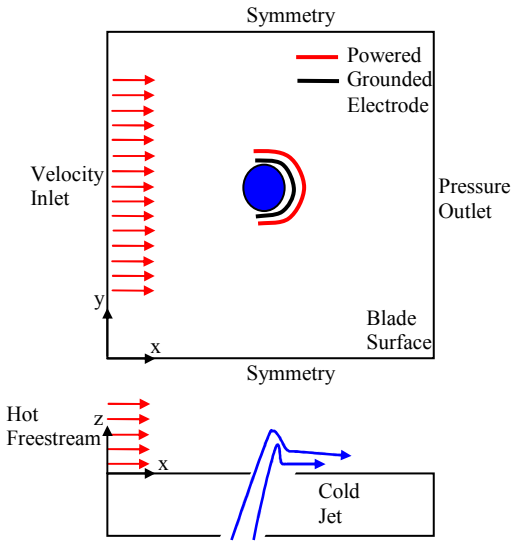


**Figure 3. Schematic shows the top view and the side view of the film cooling flow with plasma inward force.**

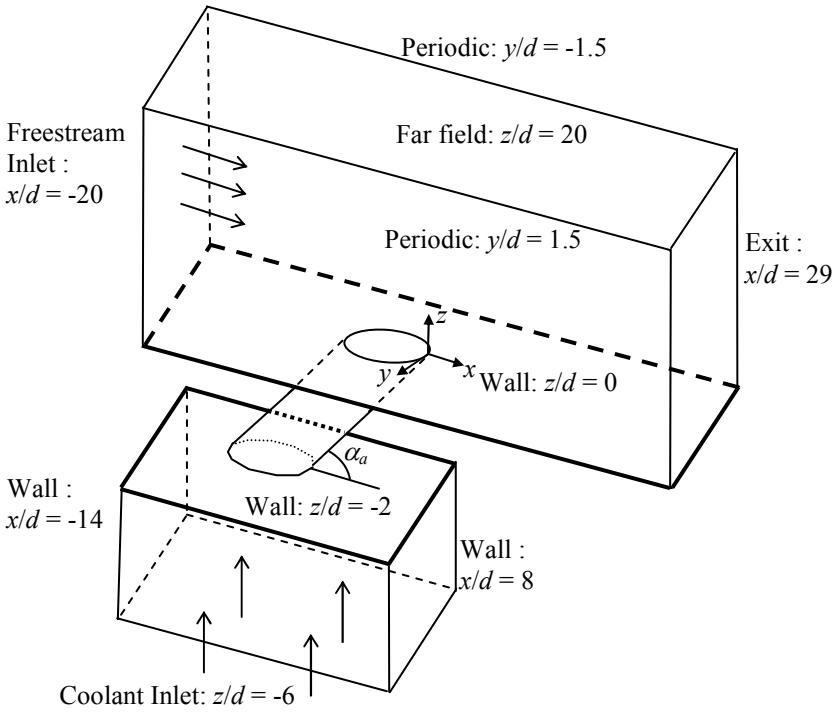


**Figure 4. Schematic shows the film cooling flow. The geometry and boundary conditions are based on reported test setup.[14]**

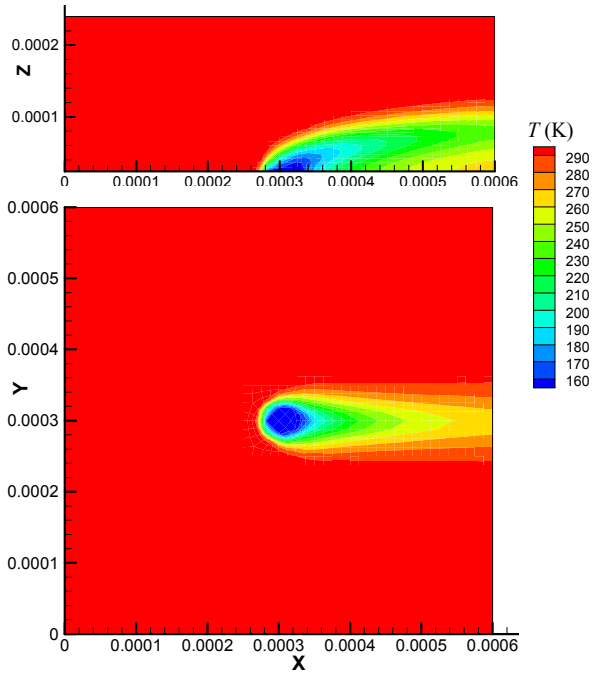


**Figure 5. Temperature distribution on the *xz*-plane of $y = 0.3$ mm and on the *xy*-plane of $z = 0.03$ mm for the test case one without plasma force.**

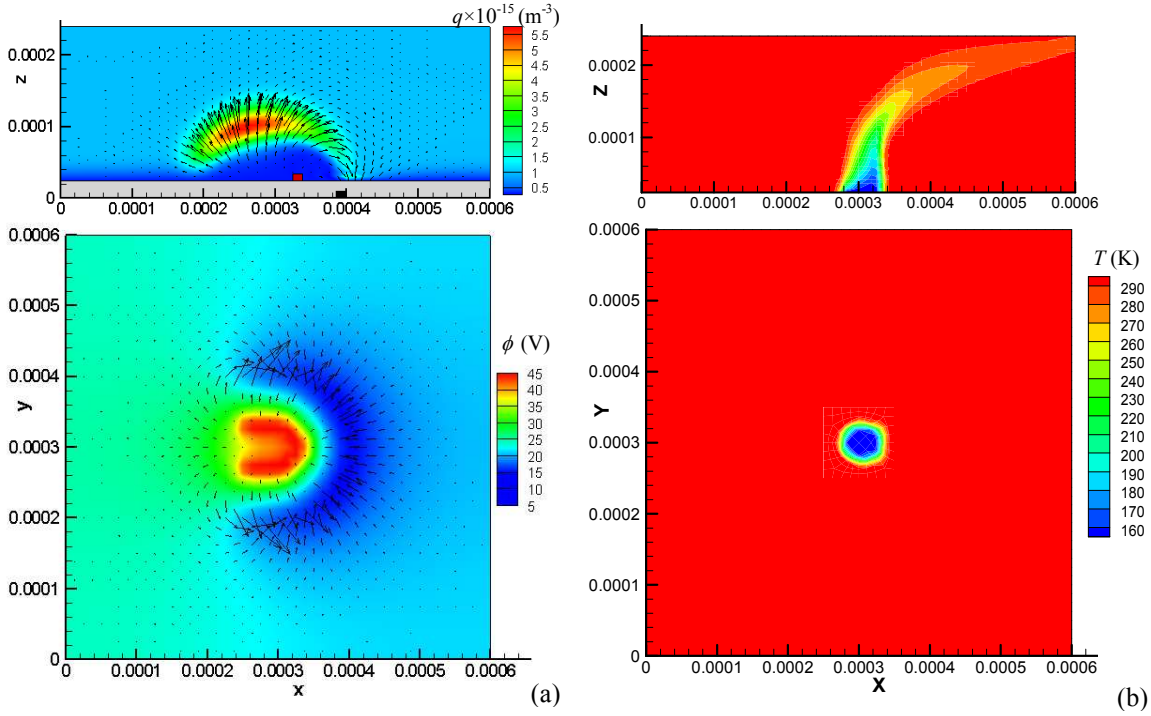


**Figure 6. Test case two with plasma outward force for (a) charge separation contour $q = n_i - n_e$ at *xz*-plane ($y = 0.3$ mm) and potential distribution at *xy*-plane ($z = 0.03$ mm) with force vectors, and (b)temperature distribution on the *xz*-plane of $y = 0.3$ mm and on the *xy*-plane of $z = 0.03$ mm.**

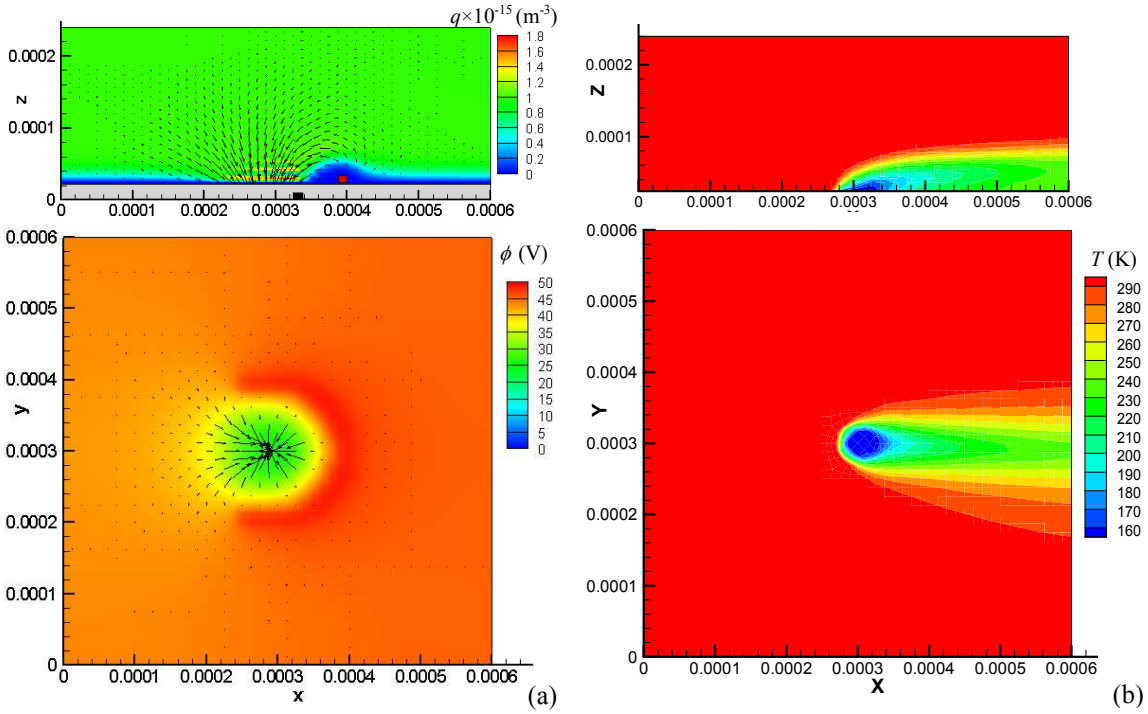


**Figure 7. Test case three with plasma inward force for (a) charge separation contour $q = n_i - n_e$ at *xz*-plane ($y = 0.3$ mm) and potential distribution at *xy*-plane ($z = 0.03$ mm) with force vectors, and (b)temperature distribution on the *xz*-plane of $y = 0.3$ mm and on the *xy*-plane of $z = 0.03$ mm.**

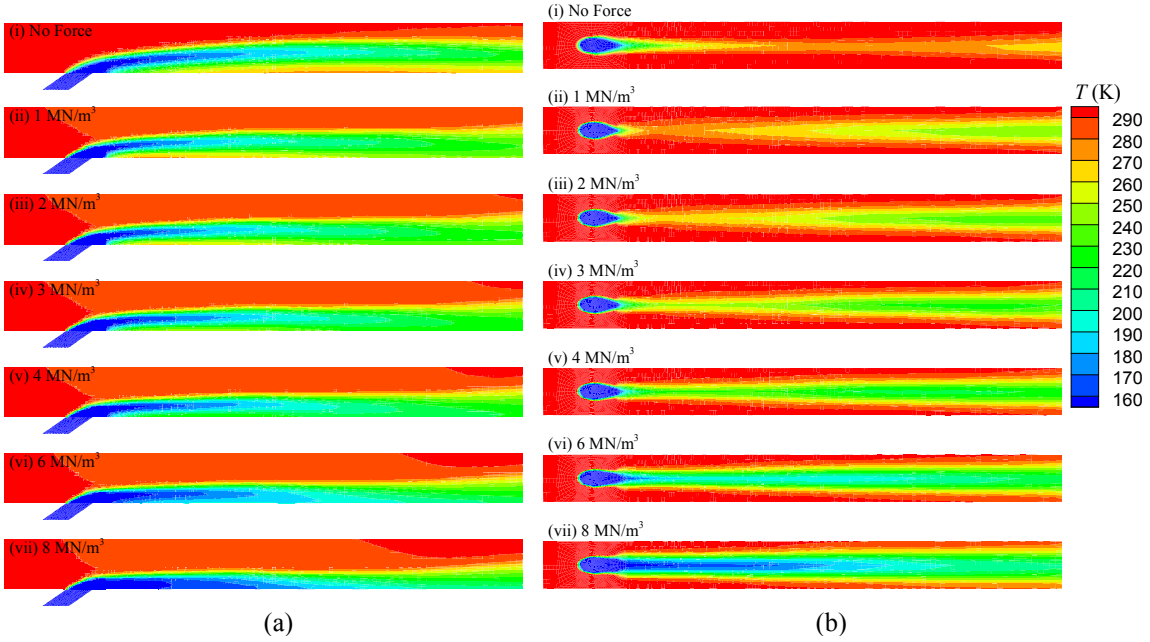


**Figure 8. Temperature contour with different force densities $F_x$ = (i) 0, (ii) 1, (iii) 2, (iv) 3, (v) 4, (vi) 6, and (vi) 8 MN/m$^3$ for (a) along the vertical plane at $y = 0$ and B) on the work surface $z = 0$.**

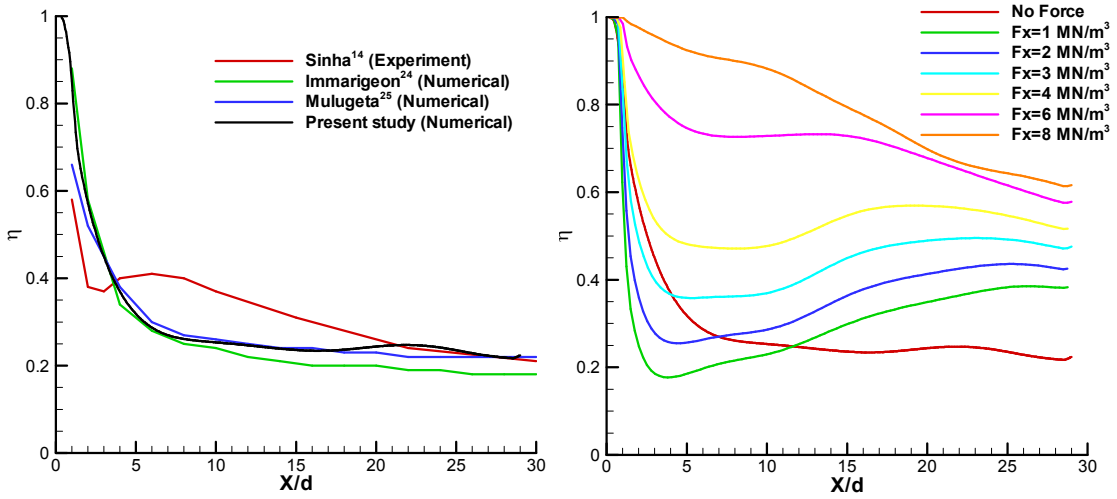


**Figure 9. Comparison of centerline effectiveness $\eta$ at downstream of coolant hole for (a) baseline case of experimental data and numerical work, and (b) plasma force varied from 0 to 8 MN/m$^3$.**